Available online at www.sciencedirect.com
ScienceDirect
International Journal of Heat and Mass Transfer 51 (2008) 1665–1674
International Journal of HEAT and MASS TRANSFER
www.elsevier.com/locate/ijhmt

Interactions of thermally induced acoustic waves with buoyancy induced flows in rectangular enclosures

Yiqiang Lin [a], Bakhtier Farouk [a,*], Elaine S. Oran [b]

[a] Department of Mechanical Engineering and Mechanics, Drexel University, Philadelphia, PA 19104, United States
[b] Laboratory for Computational Physics and Fluid Dynamics, Naval Research Laboratory, Washington, DC, United States

Received 3 November 2006; received in revised form 12 July 2007
Available online 29 August 2007

Abstract

Acoustic waves are generated when a compressible-fluid is exposed to a rapidly varying heat flux along a confining wall. For an enclosure, these waves reverberate and eventually decay. Buoyancy-induced flows generated within an enclosure can be affected by the acoustic waves generated. The interactions of the acoustic waves produced by rapid heating of a wall with the buoyancy-induced flow in air filled rectangular enclosures are investigated numerically. For the present simulations, the bottom wall of the enclosure is heated rapidly with varying heating rates, while the top wall is held at the initial temperature of the air. The vertical walls of the enclosure are considered insulated. The compressible unsteady Navier–Stokes equations are solved by an explicit flux-corrected transport algorithm for the convection terms and by a central-differencing scheme for the viscous and conduction terms.

Keywords: Thermally induced acoustic wave; Buoyancy-induced flow; Enclosure flow

1. Introduction

When a compressible-fluid within an enclosure is subjected to a rapid temperature increase along a bounding wall, the part of the fluid in the immediate vicinity of the wall expands. This results in a fast increase in the local pressure, and leads to the generation of pressure (acoustic) waves. The pressure waves propagate at nearly the sound speed of the fluid, and are repeatedly reflected from the opposing walls of the enclosure. A flow field may develop within the enclosure due to the oscillating pressure waves, and an 'acoustic wave induced' convective heat transfer mode can be introduced to the system. For fluids with low heat diffusivity values (e.g. near-critical fluids) such a convective mode of heat transport can be significant [1].

There has been a considerable amount of analytic and some related numerical and experimental work to study thermally induced pressure waves [2–10]. The problem of thermally induced waves in a quiescent semi-infinite body of a perfect gas, subjected to a step change in temperature at the solid wall has been studied analytically [11] to determine how the sound intensity depends on the history of the wall temperature. The one-dimensional compressible flow equations were linearized and a closed-form asymptotic solution was obtained using a Laplace transform technique. Solutions from a simplified model (the hyperbolic equation of conduction) for thermally induced motion was compared with one-dimensional Navier–Stokes equations model of the phenomena and limitations of the simplified approach was discussed [4]. Later a more general class of solutions for the thermally induced waves was obtained for step and gradual changes in the boundary temperature by using the Laplace transform method with a linear wave model [5]. The equations of the nonlinear wave model were numerically solved using finite-differences scheme modified with a Galerkin finite element interpolation in space. The analysis was, however. limited to a gas

* Corresponding author. Tel.: +1 215 898 2287; fax: +1 215 895 1487.
E-mail address: bfarouk@cbis.ece.drexel.edu (B. Farouk).

0017-9310/$ - see front matter © 2007 Elsevier Ltd. All rights reserved.
doi:10.1016/j.ijheatmasstransfer.2007.07.008

Nomenclature

a	acoustic speed
e	internal energy
E	total energy
g	gravitational acceleration
Gr_H	Grashof number, $\frac{g\beta(T_b-T_t)H^3}{\nu}$
$\bar{h}$	mean heat transfer coefficient
H	height of the enclosure
k	thermal conductivity
L	width of the enclosure
$\overline{Nu_H}$	mean Nusselt number, $\frac{\bar{h}H}{k}$
p	pressure
q	heat flux
R	specific gas constant
t	time
T	temperature
u	velocity component in the horizontal direction
v	velocity component in the vertical direction
x	the horizontal direction
y	the vertical direction

Greek Symbols

μ	dynamic viscosity
ρ	density
ϕ	viscous dissipation
τ	time constant for rapid heating

Subscripts

0	initial
b	bottom wall
n	normal to the wall
t	top wall
w	wall position

medium with a Prandtl number of 0.75. Thermally induced convection phenomena were experimentally investigated in a cylinder containing air with temperature measurements in normal and reduced gravity environment by Parang and Salah-Eddine [8]. Only temperature measurements were reported. Experimental measurements of the pressure waves generated by rapidly heating a surface were reported for the first time by Brown and Churchill [9].

On the other hand, buoyancy-induced convective flows inside a rectangular enclosed enclosure has been widely investigated. Buoyancy induced flows can be generated by differentially heating either the vertical walls or the horizontal walls. For differential heating of the horizontal walls, two distinct situations may arise [12]. If the upper wall is maintained at a higher temperature than the lower wall, the lower-density fluid is above the higher-density fluid and no convection currents will be experienced. The second, and more interesting case is experienced when the lower wall has higher temperature than the upper wall. The previous studies [13–15] on buoyancy-induced flows in enclosures did not consider the effect of heating rate of the wall on the development of convection and its interaction with the acoustic waves generated due to rapid heating.

Numerical studies of one- and two-dimensional thermally induced waves in a confined region were carried out by Ozoe and Churchill [16,17], Farouk et al. [3], Brown and Churchill [10] and Aktas and Farouk [18]. These computational studies described finite-difference solutions of the compressible Navier–Stokes equations for a gas with temperature-independent thermophysical properties. Ozoe and Churchill [16,17] obtained their solutions by employing the upwind scheme to solve the governing equations, and as a consequence, the results showed effects of substantial numerical diffusion. Brown and Churchill [10] had shown that rapid heating of a solid surface bounding a region of gas generates a slightly supersonic wave with positive amplitude in pressure, temperature, density and mass velocity. Using a high-order numerical scheme, Farouk et al. [3] predicted the early time behavior of thermally induced waves in a compressible-fluid filled cavity where temperature dependent fluid properties were used. The computational results agreed well with available experimental data in the literature. More recently Aktas and Farouk [18] concluded that for acoustic waves generated by a suddenly heated sidewall in a rectangular enclosure, the effect of gravitational acceleration was negligible at the early times. Lin and co-workers [19] investigated the effect of gravity on the development of flow field generated by thermally induced acoustic waves in a square enclosure. The left (side) wall of a closed enclosure was heated both impulsively and gradually such that acoustic waves of varying strengths were generated. The effect of gravity was found to have little effect on the pressure field during the early times.

In the present paper, the interactions of thermally induced acoustic waves with the buoyancy-induced flow are reported for bottom heated rectangular enclosures. We consider enclosures with varying aspect ratios with bottom heating for the present study. Enclosures with three different aspect ratios ($H/L = 0.5$, 1.0 and 5.0) were considered. The effect of the thermally induced pressure waves are expected to be stronger for enclosures with smaller values of the aspect ratio. Both bottom and top heating conditions were examined. The vertical side walls of the rectangular enclosure are considered to be insulated. Initially the gas and all walls are in thermal equilibrium ($T = T_0$ everywhere). At $t > 0$, the bottom wall temperature is increased rapidly to a value $T_b (T_b > T_0)$

$$T_b(t) = T_0[1 + \left(\frac{T_{\max} - T_0}{T_0}\right)(1 - e^{-\frac{t}{\tau}})] \quad (1)$$

while the top wall is kept at the initial temperature ($T_t = T_0$), In Eq. (1) $T_{\max}$ is the maximum temperature that the heated bottom wall can attain. The rate of increases of the bottom wall temperature can be controlled by varying the time constant τ value in Eq. (1). This is important because the temperature increase rate has significant effect on the strength of thermally induced acoustic wave, according to the pervious studies [3]. For all calculations reported in this paper, the value of $\frac{T_{\max}-T_0}{T_0}$ is set to 0.333. To study the effect of gravity on the flow field generated by thermally induced acoustic wave, the computations were carried out for different gravity conditions, viz., $+1.0g$, $0g$ and $-1.0g$.

2. Mathematical model

The development of the thermally induced wave and buoyancy-induced flow is governed by the Navier–Stokes equations for a compressible-fluid. In the two-dimension Cartesian coordinates, these equations can be expressed in the conservative form as

$$\frac{\partial \rho}{\partial t} + \frac{\partial(\rho u)}{\partial x} + \frac{\partial(\rho v)}{\partial y} = 0 \quad (2)$$

$$\frac{\partial(\rho u)}{\partial t} + \frac{\partial(\rho u^2)}{\partial x} + \frac{\partial(\rho uv)}{\partial y} + \frac{\partial p}{\partial x} = \frac{\partial \tau_{xx}}{\partial x} + \frac{\partial \tau_{xy}}{\partial y} \quad (3)$$

$$\frac{\partial(\rho v)}{\partial t} + \frac{\partial(\rho uv)}{\partial x} + \frac{\partial(\rho v^2)}{\partial y} + \frac{\partial p}{\partial y} = \frac{\partial \tau_{xy}}{\partial x} + \frac{\partial \tau_{yy}}{\partial y} - \rho\zeta \quad (4)$$

$$\frac{\partial E}{\partial t} + \frac{\partial(Eu)}{\partial x} + \frac{\partial(Ev)}{\partial y} + \frac{\partial(pu)}{\partial x} + \frac{\partial(pv)}{\partial y} = \frac{\partial q_x}{\partial x} + \frac{\partial q_y}{\partial y} + \phi \quad (5)$$

where ρ is the density, u and v are the velocity components, E is the total energy, and p is the pressure. For normal, reversed and zero-gravity conditions, $\zeta = 1.0g$, $-1.0g$ or 0, respectively.

The stress tensor τ_{ij} can be written as

$$\tau_{xx} = 2\mu\frac{\partial u}{\partial x} - \frac{2}{3}\mu\left(\frac{\partial u}{\partial x} + \frac{\partial v}{\partial y}\right) \quad (6)$$

$$\tau_{yy} = 2\mu\frac{\partial v}{\partial y} - \frac{2}{3}\mu\left(\frac{\partial u}{\partial x} + \frac{\partial v}{\partial y}\right) \quad (7)$$

$$\tau_{xy} = \tau_{yx} = \mu\left(\frac{\partial v}{\partial x} + \frac{\partial u}{\partial y}\right) \quad (8)$$

where μ is the dynamic viscosity.

The components of the heat flux are written as

$$q_x = \lambda\frac{\partial T}{\partial x} \quad (9a)$$

$$q_y = \lambda\frac{\partial T}{\partial y} \quad (9b)$$

where λ is the thermal conductivity and T is the temperature.

Table 1
List of computational cases

	L (m)	H/L	Heating rate τ (s)	Gr_H	Gravity ζ
1	0.02	1.0	5.76×10^{-5}	5.27×10^{4}	$+1.0g$
2	0.02	1.0	5.76×10^{-5}	–	$0g$
3	0.02	1.0	5.76×10^{-5}	-5.27×10^{4}	$-1.0g$
4	0.02	1.0	2.88×10^{-4}	5.27×10^{4}	$+1.0g$
5	0.02	1.0	1.15×10^{-2}	5.27×10^{4}	$+1.0g$
6	0.02	0.5	5.76×10^{-5}	6586	$+1.0g$
7	0.02	5.0	5.76×10^{-5}	6.59×10^{6}	$+1.0g$

The viscous dissipation in Eq. (5) is written as

$$\phi = \frac{\partial(\tau_{xx}u + \tau_{xy}v)}{\partial x} + \frac{\partial(\tau_{yx}u + \tau_{yy}v)}{\partial y} \quad (10)$$

In addition, an equation of state for perfect gas is used to relate the air temperature to the other thermodynamic properties

$$p = \rho PT \quad (11)$$

3. Numerical scheme

The governing equations (except for the diffusion terms) are discretized using a control-volume-based finite-volume method based on the flux-corrected transport (FCT) algorithm. FCT is a high-order, nonlinear, monotone, conservative and positivity-preserving scheme designed to solve a general one-dimensional continuity equation with appropriate source terms. This scheme has fourth-order phase accuracy and is able to resolve steep gradients with minimum numerical diffusion. In this algorithm, when a flow variable such as a density is initially positive, it remains positive during the computations and no new minimum or maximum values are introduced due to numerical errors in the calculation process. To ensure positivity and stability, a minimum amount of numerical diffusion over the stability limit is added at each time-step. Time-step splitting technique is used to solve the two-dimensional problem

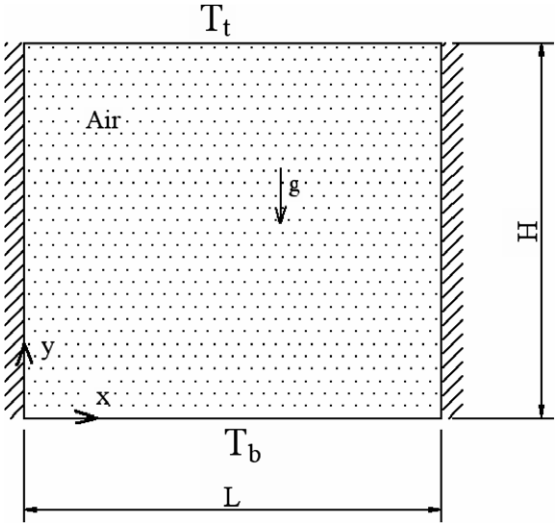

Fig. 1. Geometry and boundary conditions of the problem.

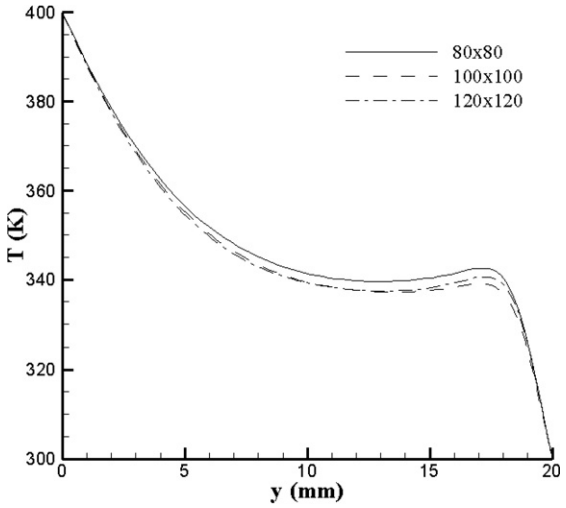

Fig. 2. Variation of temperature with y along the horizontal mid-plane of the enclosure at $t = 1.27$ s ($H/L = 1, \tau = 5.76 \times 10^{-5}$ s, $+1.0g$), for different grid sizes.

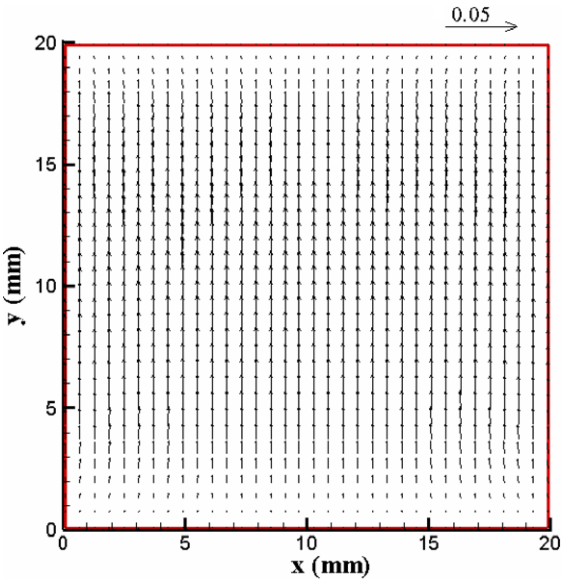

Fig. 4. Velocity vectors at $t = 0.058$ s ($H/L = 1, \tau = 5.76 \times 1^{-5}$ s), $1.0g$, case 1 (no significant variations for $0g$ and $-1.0g$ conditions, cases 2 and 3).

addressed here. Further details of the FCT algorithm used here are documented in [20]. The diffusion terms (the viscous term in the momentum equations and the conduction terms in the energy equation) were discretized using the central-difference approach and the time-step splitting technique was used to include the terms in the numerical scheme. Time-step splitting technique was also used to include the gravity term in the y-momentum equation and the viscous dissipation terms in the energy equation.

The time-steps for explicit methods are restricted due to the stability requirements. It is calculated by [20],

$$\Delta t = (\mathrm{CFL}) \cdot \min\left[\frac{\min(\Delta x_{i,j}, \Delta y_{i,Sj})}{a_{i,j}}\right] \tag{12}$$

where CFL represents the Courant–Friedrichs and Lewy number. For each new time-step, the above equation is evaluated over the entire grid. For the present calculations, the CFL number is limited to be less than one-half. A value of 0.4 is used for all calculations.

No slip boundary conditions were used for all the solid walls. A high-order non-dissipative algorithm such as FCT requires rigorous formulation of the density boundary conditions. Otherwise, numerical solutions may show spurious wave reflections at the regions close to boundaries and non-physical oscillations arising from instabilities. In the present computational method, the treatment proposed by Poinsot and Lele [21] was followed for implementing the boundary conditions for the density. Along any solid wall, the density is calculated from

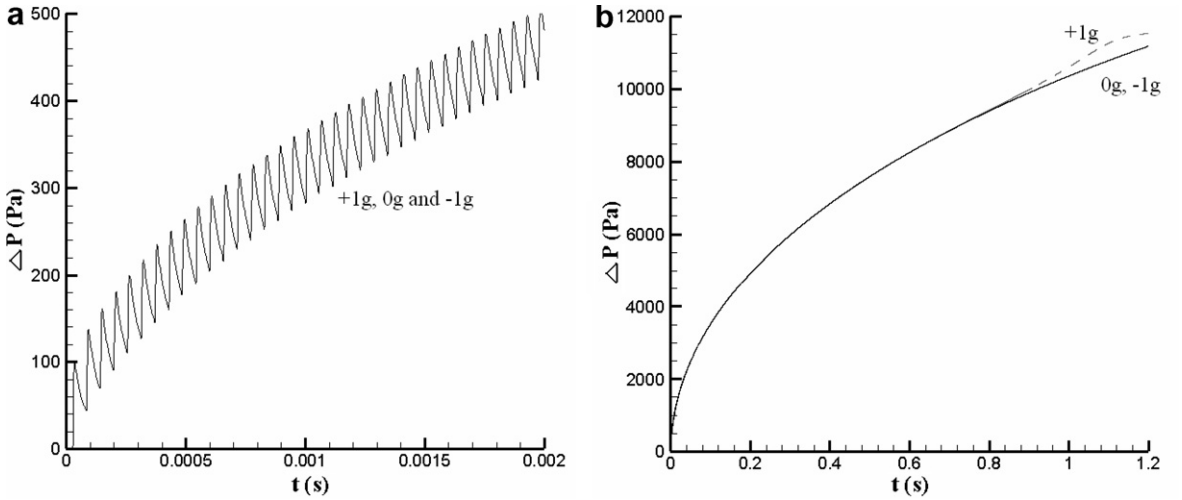

Fig. 3. Variation of pressure ($p - p_i$) with time at the midpoint of the enclosure ($H/L = 1, \tau = 5.76 \times 10^{-5}$ s), for different gravity conditions ($+1.0g$, $0g$ and $-1.0g$), cases 1–3 (a) early time and (b) long time.

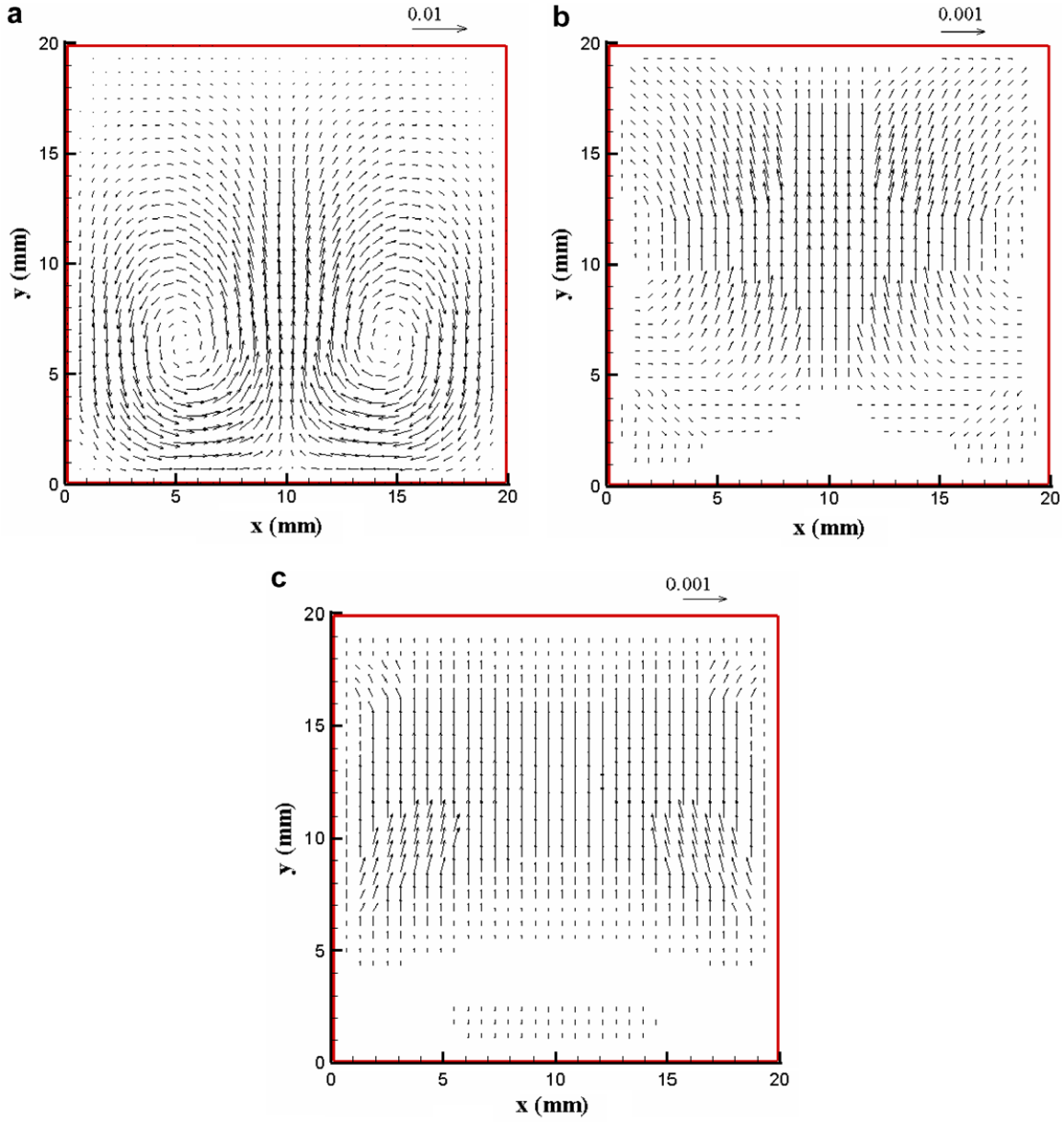

Fig. 5. Velocity vectors at $t = 0.58$ s ($H/L = 1, \tau = 5.76 \times 10^{-5}$ s), (a) $+1.0g$, case 1 (b) $0g$, case 2 (c) $-1.0g$, case 3.

$$\left(\frac{\partial \rho}{\partial t}\right)_{\mathrm{w}} + \frac{1}{a_{\mathrm{w}}}\left(\frac{\partial \rho}{\partial n} + \rho a_{\mathrm{w}} \frac{\partial u_n}{\partial n}\right)_{\mathrm{w}} = 0 \tag{13}$$

where the subscript w signifies the location of the wall, and n is the direction normal to the wall.

4. Results and discussion

Numerical simulations of thermally induced wave and buoyancy-induced flow were performed in a rectangular enclosure filled with air. The initial pressure of air is 1 atm, and the initial temperature (T_0) is 300 K. The bottom wall is heated to 400 K ($T_{\max}$) at different heating rates (Eq. (1), varying τ), while the top wall is kept at the initial temperature. Results were obtained for seven cases (Table 1) to study the effects of gravity, heating rate, and aspect ratio (H/L) on the flow field and the heat transfer characteristics. For all cases studied, the width of the enclosure was considered to be $L = 0.02$ m.

Results of a prior investigation by Farouk et al. [3] considered the short-time behavior of the thermoacoustic waves generated by impulsive and gradual heating of a wall. The results were in very good qualitative and quantitative agreement with those given in the literature. In the present study, longer-time behavior of the temperature and velocity fields produced by rapid heating of the bottom wall, was investigated under zero and normal gravity conditions (Fig. 1).

For a mesh-resolution study, the computational results for the variation of temperature with y at the vertical

midplane using three different mesh sizes, 80×80, 100×100 and 120×120, are shown in Fig. 2 for case 1 (see Table 1) at t =1.27 s. The time step (2.81×10^{-8} s) was, however, the same for all three mesh sizes. From this figure, a mesh size of 100 × 100 was found to be adequate for the present computations for cases with $H/L = 1.0$. For cases with non-unity aspect ratios (Table 1) the mesh sizes were adjusted such that grid density is approximately the same as found in case 1.

In the following sections, we discuss the effects of gravity, effects of the heating rate and the effects of the aspect ratio of the enclosure on the flow and temperature fields generated by sudden heating of the bottom wall of the enclosure.

4.1. Effect of gravity

Simulations were carried out for identical conditions with three different values of the parameter ζ, (Eq. (4)) viz., $+1.0g$, $0g$, and $-1.0g$ (cases 1, 2 and 3, respectively). The aspect ratio of the enclosure is fixed at 1.0 for all of the above three cases, and the time constant of the heating process τ is also kept at 5.76×10^{-5} s. This value is represents the time for an acoustic wave to travel from the bottom of the enclosure ($H = 0.02$ m) to the top under normal atmospheric conditions.

The predicted variations of pressure at the midpoint of the enclosure for all three cases are shown in Figs. 3a and b. A distinctive peak is observed whenever the thermal induced pressure wave crosses the midpoint. This wave traveling at slightly supersonic speed, periodically reflects from both side walls as seen by the multiple peaks. The shapes of the pressure wave are also found to be nearly same for the different gravity conditions at early time (Fig. 3a). The pressure variations are plotted over a larger time-scale in Fig. 3b and the oscillations shown in Fig. 3a are not noticeable in the figure anymore due to the change of scale in the pressure axis. For all three cases, the pressure rise behavior is identical. Minor differences only show up when the slower response buoyancy-induced flow starts developing at larger times for case 1 (Fig. 3b). For case 1, the center point is at the middle of a developing vortical flow, thus causing the incipient pressure rise.

The velocity vectors in Fig. 4 show the flow field developed from the wave motion created by the rapid heating of the bottom wall at an early time ($t = 0.058$ s) for case 1. Due to spatially uniform heating, the flow field is essentially symmetric along the vertical middle-plane. Flow structures develop along the top and bottom corners due

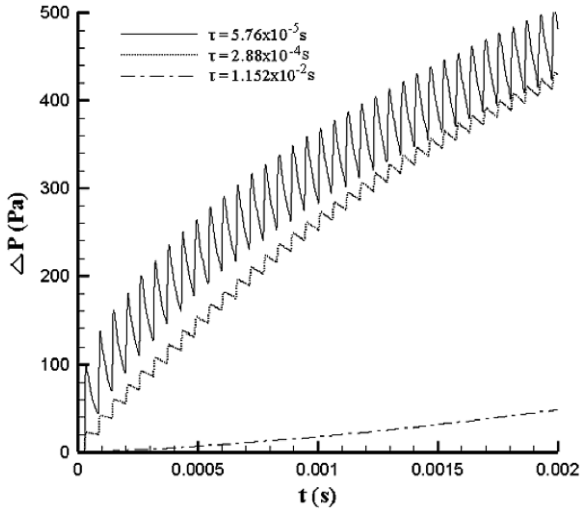

Fig. 7. Variation of pressure with time at the midpoint of the enclosure ($H/L = 1.0$, $+1.0g$), under different heating rates, cases 1, 4 and 5.

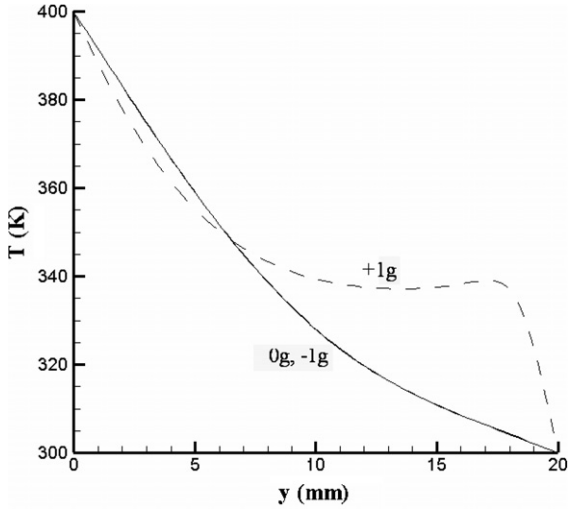

Fig. 6. Variation of temperature with y at the midpoint of the enclosure at $t = 1.27$ s ($H/L = 1, \tau = 5.76 \times 10^{-5}$ s), under different gravity conditions, cases 1–3.

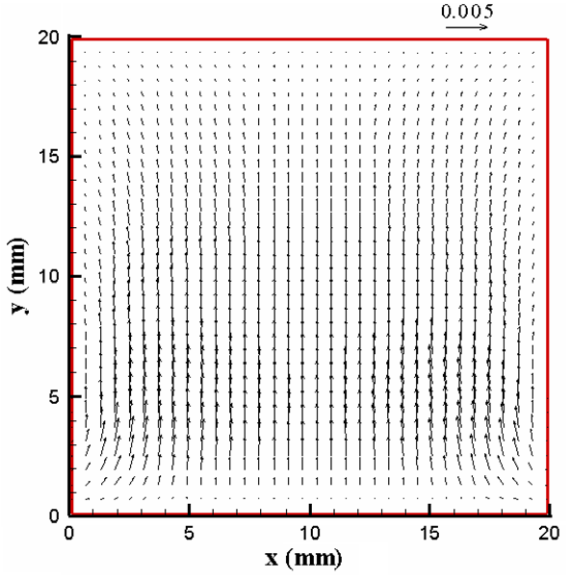

Fig. 8. Velocity vectors at $t = 0.058$ s ($H/L = 1$, $+1g$), under heating rate $\tau = 1.15 \times 10^{-2}$ s, case 5.

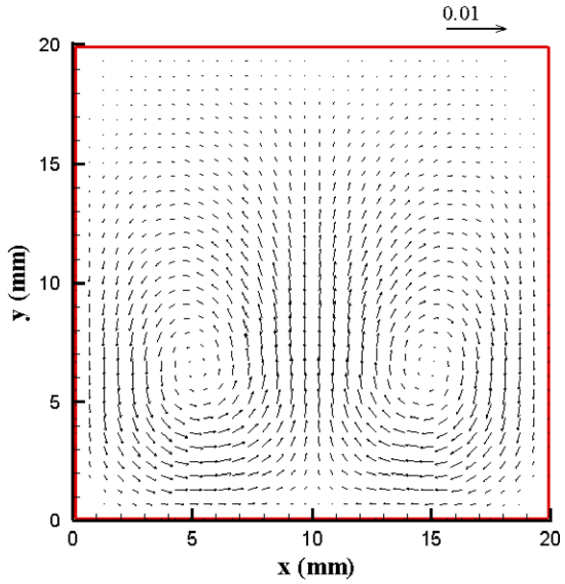

Fig. 9. Velocity vectors at $t = 0.58$ s ($H/L = 1.0$, $+1g$), under heating rate $\tau = 1.15 \times 10^{-2}$ s, case 5.

to viscous interactions between the solid surfaces and bulk fluid. Similar results for cases 2 and 3 (at $t = 0.058$ s) show essentially no difference with those shown in Fig. 4. The flow fields at a larger time ($t = 0.58$ s), however, start showing the distinct effects of gravity on the acoustic wave induced flow field, as shown in Figs. 5a, b and c for cases 1, 2 and 3, respectively. For the case of $+1.0g$ two characteristic eddies are formed due to the buoyancy-induced flow. For the cases of $0g$, Fig. 5b and $-1.0g$, Fig. 5c, the flow fields generated by the acoustic waves are considerably damped, due to viscous dissipation. The dampening is further enhanced by the stratified density field that is created in the opposed gravity ($-1.0g$) case.

Fig. 6 shows the instantaneous temperature profiles along the vertical mid-plane for cases 1, 2 and 3 at $t = 1.27$ s. In the cases of $0g$ (case 2) and $-1.0g$ (case 3), the temperature profiles tend to be nearly linear, because heat conduction and acoustic compression and rarefaction influence the temperature distribution (no recirculating flow development). However, for the case of $+1.0g$ (case 1), sharp temperature gradients are observed near the two horizontal walls and an inversion to the temperature profile is obtained near the middle of the enclosure due to a developing vortical flow.

4.2. Effect of heating rate

Next we studied the effect of heating rate (as characterized by the value of τ in Eq. (1)). Simulations were carried out for varying values of τ: 5.76×10^{-5}, 2.88×10^{-4}, and 1.15×10^{-2} as shown in Table 1 (cases 1, 4 and 5, respectively). The aspect ratio of the enclosure is fixed at 1.0 and the value of $\zeta = +1.0g$ for all three cases.

The variation of pressure at the midpoint of the enclosure is shown in Fig. 7 for cases 1, 4 and 5. The strength of the pressure wave and the overall rate of pressure increase are found to be strongly related to the heating rate. The acoustic waves produced are rather weak when the heating rate is slower as in case 5 ($\tau = 1.15 \times 10^{-2}$ s), compared to case 1 ($\tau = 5.7 \times 10^{-5}$ s) and case 4 ($\tau = 2.88 \times 10^{-4}$ s).

For $\tau = 1.15 \times 10^{-2}$ s, the development of flow fields at $t = 0.058$ s is shown in Fig. 8. At this early time, the fluid motion is limited to the vertical direction as dictated by the acoustic waves. Comparing the results shown in

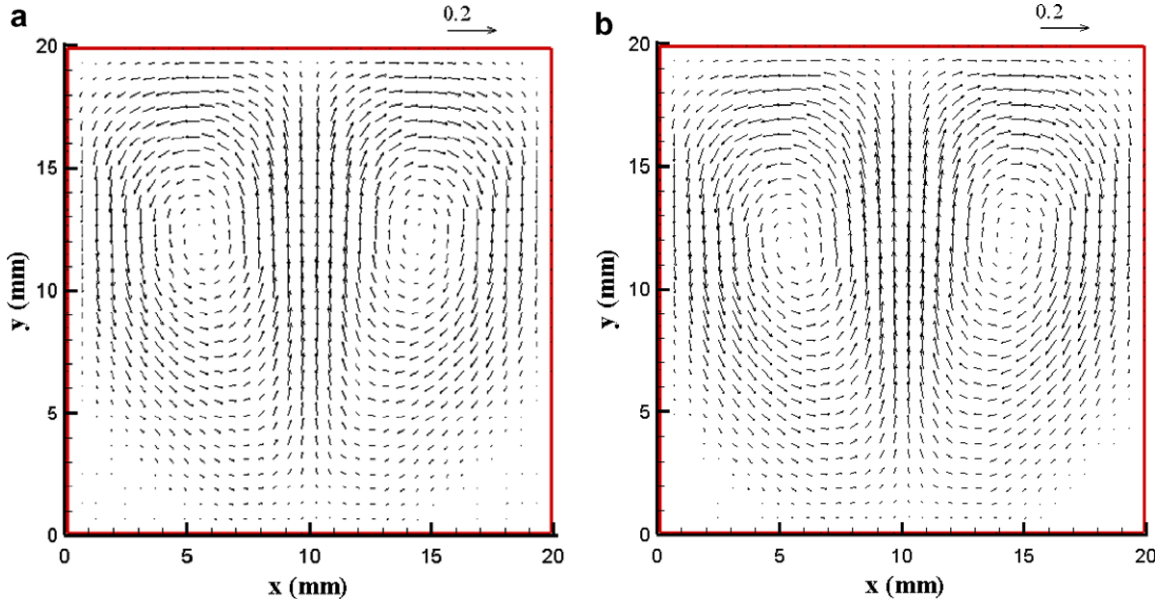

Fig. 10. Velocity vectors at $t = 1.27$ s ($H/L = 1.0$, $+1$g), under varying heating rates (a) $\tau = 5.76 \times 10^{-5}$ s, case 1 (b) $\tau = 1.15 \times 10^{-2}$ s, case 5.

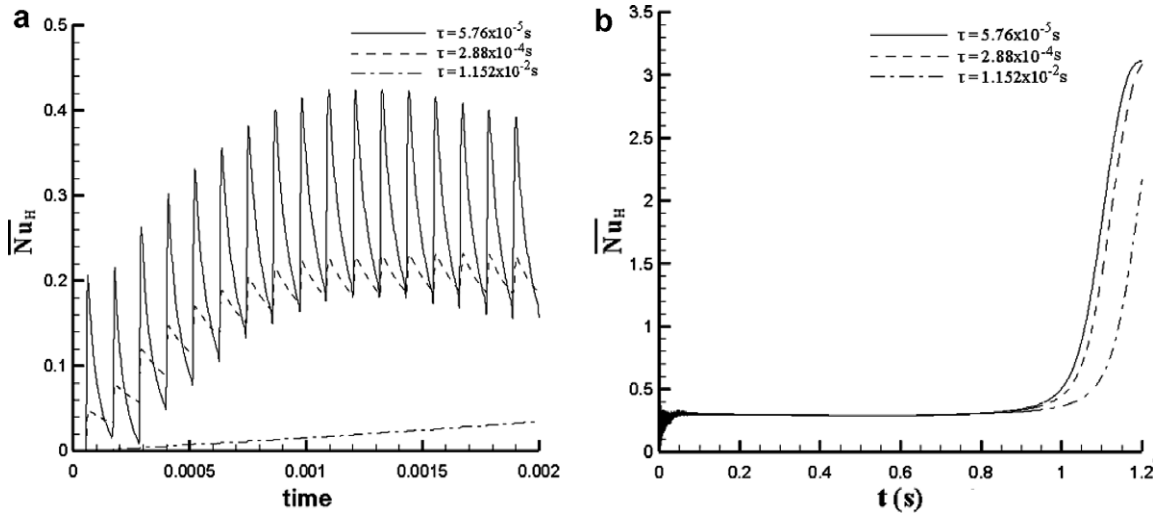

Fig. 11. Variation of $\overline{Nu_H}$ with time at the top wall ($H/L = 1.0$, $+1.0g$), under different heating rates, cases 1, 4 and 5. (a) early time and (b) long time.

Fig. 8 to those shown in Fig. 4 ($\tau = 5.76 \times 10^{-5}$, case 1), the strength of the flow field is found to be considerably weaker when the time constant of the heating rate is increased from 5.76×10^{-5} s (case 1) to 1.15×10^{-2} s (case 5). At early times for both values of τ, the flow field is dominated by the thermally induced pressure field and no buoyancy effects are evident.

Fig. 9 shows the development of velocity vectors at $t = 0.5$ s for case 5. The flow field begins to show the signs of a developing buoyancy-induced flow. Two eddies are found to form near the bottom wall. Compared to similar results (Fig. 5a), for case 1, the velocity values are somewhat lower in case 5 (Fig. 9). The strong acoustically induced flowfield in case 1 inhibits the initial development of the buoyancy-induced flowfield in case 1. The flow fields for case 1 and case 5 will eventually be identical, as the acoustic waves damp out as shown in Figs. 10a and b, at $t = 1.27$ s.

The effect of the heating rate on the variation of heat transfer along the top wall is shown in Figs. 11a and b for cases 1, 4 and 5. At the early time, Fig. 11a, the spatially averaged $\overline{Nu_H}$ along the top wall fluctuates with time due to the thermally induced pressure waves, which is stronger for faster heating rate (lower time constant τ). At larger time, Fig. 11b, the fluctuations damp out, but $\overline{Nu_H}$ is still highest for the fastest heating rate, case 1. The $\overline{Nu_H}$ for all three heating rates will become identical when the acoustic waves completely damp out.

Time variation of the spatially averaged $\overline{Nu_H}$ (t) along the top and bottom walls are given in Fig. 12 for case 1 for a period of 3 s. Initially heat transfer rate is very high along the bottom wall (heated) due to the large temperature difference between the wall and the gas. Although fully developed conditions are not established by $t = 3$ s, the results indicate that a steady state value of $\overline{Nu_H}$ will be close to 3.0. As a validation for the numerical model, one of the popular heat transfer correlations for a bottom heated closed enclosure is used to calculate the heat transfer coefficient [12],

$$\overline{Nu_H} = 0.212(Gr_H \cdot Pr)^{1/4} \tag{14}$$

for $7000 < (Gr_H \cdot Pr)^{1/4} < 3.2 \times 10^5$.

From the above correlation $\overline{Nu_H} = 2.94$ for case 1, which is close to the computed numerical results (for the top and the bottom walls) as shown in Fig. 12.

4.3. Effect of aspect ratio

Simulations were carried out for varying values of the aspect ratio $H/L = 1.0$, 0.5 and 5.0 as shown in Table 1 (cases 1, 6 and 7, respectively). The time constant of the

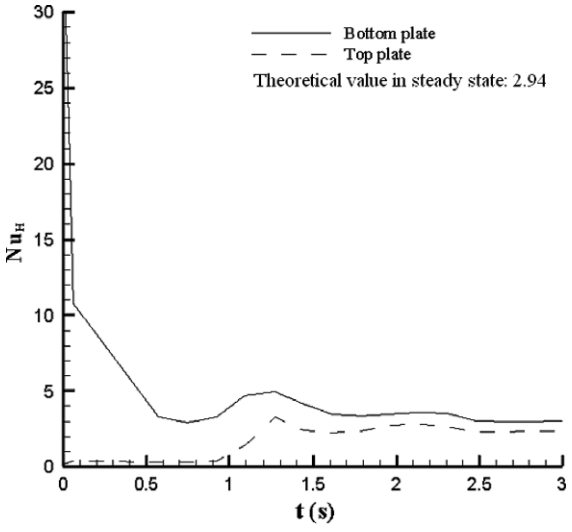

Fig. 12. Variation of $\overline{Nu_H}$ with time ($H/L = 1.0$, $+1.0g$, and $\tau = 5.76 \times 10^{-5}$ s).

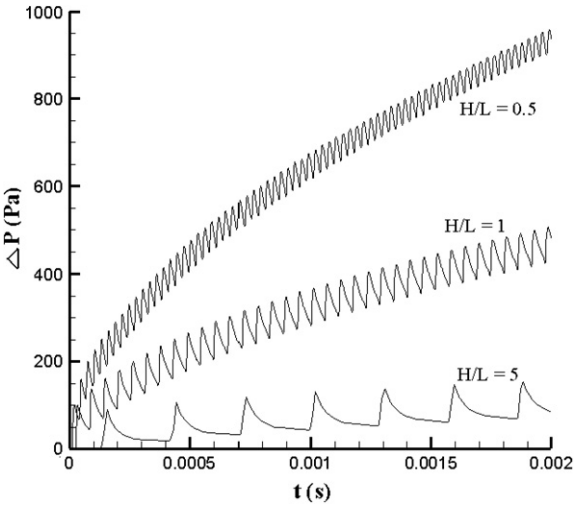

Fig. 13. Variation of pressure with time at the midpoint of the enclosure ($\tau = 5.76 \times 10^{-5}$ s, $+1g$), under different aspect ratios, cases 1, 6 and 7.

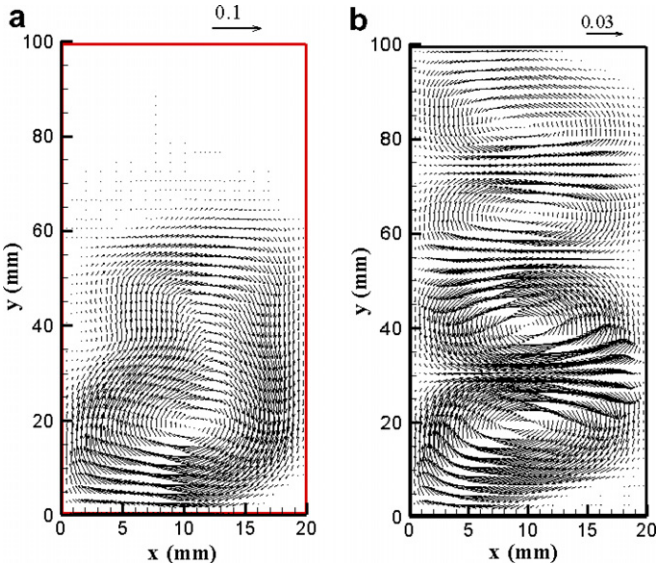

Fig. 15. Velocity vectors for $H/L = 5$, case 7, $\tau = 5.76 \times 10^{-5}$ s, $+1.0g$, (a) $t = 3.8$ s (b) $t = 7.02$ s.

heating rate $\tau = .76 \times 10^{-5}$ s and the value of $\zeta = +1.0$ g for all three cases.

The early time variation of pressure at the midpoint of the enclosures is shown in Fig. 13 for cases 1, 6 and 7. For an enclosure with the smallest aspect ratio ($H/L = 0.5$) case 6, the acoustic waves reverberate in the enclosure with a higher frequency and the pressure increase at the midpoint is rapid. For larger aspect ratios, the above frequency decreases with the rate of increase of pressure at the midpoint of the enclosure.

The flow fields at $t = 1.27$ s for cases 6 and 7 (having non-unity aspect ratio) are shown in Figs. 14a and b. The corresponding plot for case 1 was shown earlier in Fig. 10a. In all cases, two eddies created by the buoyancy-induced flow form near the bottom wall. In the case of $H/L = 5$ (case 7) the eddies affect only the lower part of the computational domain. For the tall enclosure, the flowfield was computed for an extended time. The velocity fields at $t = 3.8$ s and 7.02 s are shown in Fig. 15 for case 7. A multicellular flow field develops for this case. The multicellular structure also how periodicity along the vertical direction.

Finally, the effect of enclosure aspect ratio on the spatially averaged heat transfer coefficient $\bar{h}$ along the top wall is shown in Fig. 16. The heat transfer coefficient $\bar{h}$ along the top wall is highest for $H/L = 0.5$ and lowest for case of $H/L = 5$, where the buoyancy-induced flow field is yet to affect the top wall. The temporal variation of $\bar{h}$ for the cases 6 and 1 show interesting maxima values. For case 1, the $\bar{h}$ value increases sharply near $t = 1.0$ s which is characterized by the development of the two eddies that bring warm fluid to the cold upper wall. For case 6, $H/L = 0.5$, the increase

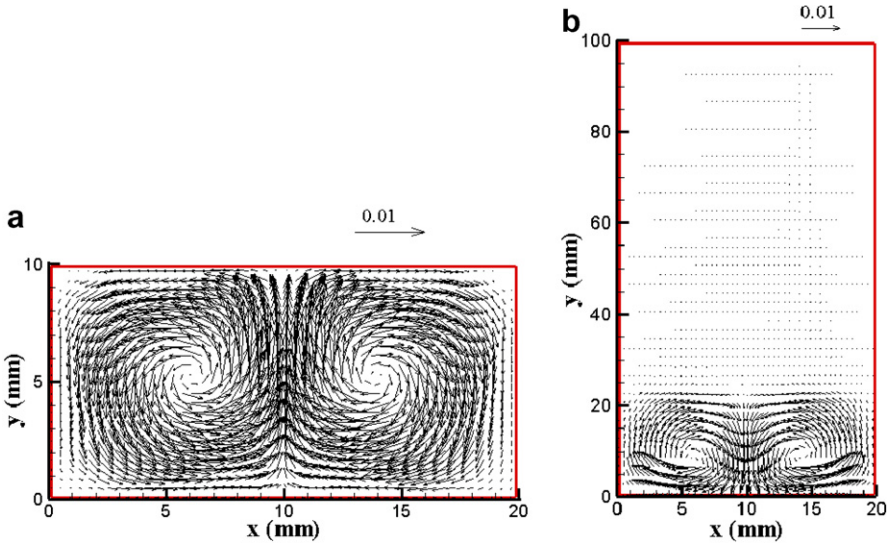

Fig. 14. Velocity vectors at $t = 1.27$ s ($\tau = 5.76 \times 10^{-5}$ s, $+1g$), under different aspect ratios (a) $H/L = 0.5$, case 6 (b) $H/L = 5.0$, case 7.

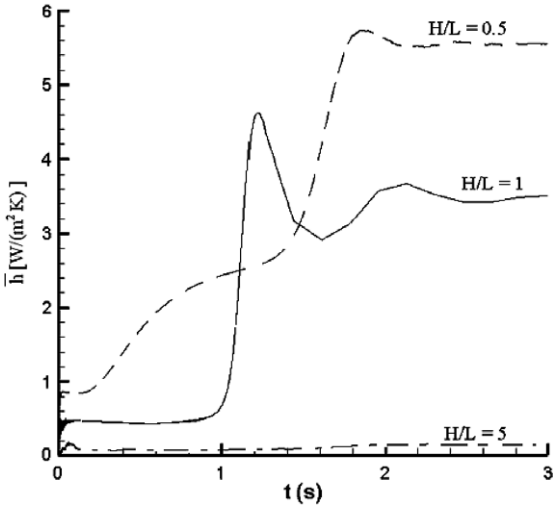

Fig. 16. Variation of $\bar{h}$ with time at the top wall ($\tau = 5.76 \times 10^{-5}$ s, $+1g$), under different aspect ratios, cases 1, 6 and 7.

of the $\bar{h}$ value is rapid as the strength of the eddies continuously bring warm fluid to the cold top wall.

5. Conclusions

Interaction of the flow fields in an enclosure generated by the acoustic waves (created by rapid heating of the bottom wall) and the buoyancy effects were studied by solving the unsteady compressible Navier–Stokes equations. The complex flow fields were simulated by using a highly accurate flux-corrected transport (FCT) algorithm. The rapidity of the wall heating process is directly proportional to the strength of the pressure waves induced. The thermally induced waves create an essentially one-dimensional oscillatory flow in the enclosure flow field. The thermally induced pressure waves eventually damp out with time. The buoyancy-induced flow is developed slowly (compared to the acoustic wave induced flows). In addition, for enclosures with low aspect ratios (H/L), the strength of the thermally induced waves has significant effects on the temporal development of the buoyancy-induced flow. It is observed that the thermally generated flow field and the buoyancy-induced flow field are both affected by the aspect ratio of the enclosure.

Acknowledgement

The authors gratefully acknowledge support from NASA grants NNC04AA22A and NNC04IA09I.

References

[1] B. Zappoli, S. Amiroudine, P. Carles, J. Ouazzani, Thermoacoustic and buoyancy-driven transport in a square side-heated cavity filled with a near-critical fluid, J. Fluid Mech. 316 (1996) 53–72.
[2] S.W. Churchill, M.A. Brown, Thermoacoustic convection and the hyperbolic equation of conduction, Int. Commun. Heat Mass 14 (1987) 647–655.
[3] B. Farouk, E.S. Oran, T. Fusegi, Numerical study of thermoacoustic waves in an enclosure, Phys. Fluids 12 (5) (2000) 1052–1061.
[4] Y. Huang, H.H. Bau, Thermoacoustic waves in a semi-infinite medium, Int. J. Heat Mass 38 (8) (1995) 1329–1345.
[5] Y. Huang, H.H. Bau, Thermoacoustic waves in a confined medium, Int. J. Heat Mass 40 (2) (1997) 407–419.
[6] M. Parang, An experimental and analytical investigation of thermoacoustic convection heat transfer in gravity and zero-gravity environments, 1986, NASA Final Report, Grant Number NAG3-239.
[7] M. Parang and Salah_Eddine, Experiments on thermoacoustic convection heat transfer in gravity and low gravity environments, Paper AIAA-87-1651, AIAA Thermophysics Conference, Honolulu, Hawaii, 1987.
[8] M. Parang, A. Salah-Eddine, Thermoacoustic convection heat-transfer phenomenon, AIAA J. 22 (7) (1984) 1020–1022.
[9] M.A. Brown, S.W. Churchill, Experimental measurements of pressure waves generated by impulsive heating of a surface, AICHE J. 41 (2) (1995) 205–213.
[10] M.A. Brown, S.W. Churchill, Finite-difference computation of the wave motion generated in a gas by a rapid increase in the bounding temperature, Comput. Chem. Eng. 23 (1999) 357–376.
[11] L. Trilling, On thermally induced sound fields, J. Acoust. Soc. Am. 27 (3) (1955) 425–431.
[12] J.P. Holman, Heat Transfer, Mc-Graw Hill, 2002.
[13] W.H. Leong, K.G.T. Hollands, A.P. Brunger, On a physically-realizable benchmark problem in internal natureal convection, Int. J. Heat Mass 41 (1998) 3817–3828.
[14] J.M. McDonough, I. Catton, A mixed finite difference-galerkin procedure for two-dimensional convection in a square box, Int. J. Heat Mass 25 (8) (1982) 1137–1146.
[15] H. Ozoe, H. Sayama, S.W. Churchill, Natural convection in an inclined square channel, Int. J. Heat Mass 17 (1974) 401–406.
[16] H. Ozoe, N. Sato, S.W. Churchill, The effect of various parameters on thermoacoustic convection, Chem. Eng. Commun. 5 (1980) 203–221.
[17] H. Ozoe, N. Sato, S.W. Churchill, Numerical analyses of two and three dimensional thermoacoustic convection generated by a transient step in the temperature of one wall, Numer. Heat Tr. A 18 (1990) 1–15.
[18] M.K. Aktas, B. Farouk, Numerical simulation of developing natural convection in an enclosure due to rapid heating, Int. J. Heat Mass 46 (2003) 2253–2261.
[19] Y. Lin, B. Farouk, E.S. Oran, Flows induced by thermoacoustic waves in an enclosure: effects of gravity, J. Thermophys. Heat Tr. 20 (3) (2006) 376–383.
[20] J.P. Boris, A.M. Landsberg, E.S. Oran, J.H. Gardner, LCPFCT- A Flux-corrected Transport Algorithm for Solving Generalized Continuity Equations, Naval Research Laboratory, Washington, DC, 1993.
[21] T.J. Poinsot, S.K. Lele, Boundary conditions for direct simulations of compressible viscous flows, J. Comput. Phys. 101 (1992) 104–129.